ACS APPLIED MATERIALS & INTERFACES

Forum Article

www.acsami.org

Polydopamine-like Coatings as Payload Gatekeepers for Mesoporous Silica Nanoparticles

Miguel-Ángel Moreno-Villaécija,[†] Josep Sedó-Vegara,[†] Eduardo Guisasola,[‡,§] Alejandro Baeza,[‡,§] María Vallet Regí,[‡,§] Fabiana Nador,[*,∥] and Daniel Ruiz-Molina[*,†]

[†]Catalan Institute of Nanoscience and Nanotechnology (ICN2), CSIC and The Barcelona Institute of Science and Technology (BIST), ICN2 Building, Campus UAB, Bellaterra, 08193 Barcelona, Spain

[‡]Departamento Química Inorgánica y Bioinorgánica, Instituto de Investigación Sanitaria Hospital 12 de Octubre i+12, Universidad Complutense de Madrid (UCM), Plaza Ramon y Cajal s/n, 28029 Madrid, Spain

[§]Centro de Investigación Biomédica en Red de Bioingeniería, Biomateriales y Nanomedicina (CIBER-BBN), Avenida Monforte de Lemos, 3−5, Pabellón 11, Planta 0, 28029 Madrid, Spain

[∥]Instituto de Química del Sur (INQUISUR-CONICET), Departamento de Química, Universidad Nacional del Sur, Avenida Alem 1253, 8000 Bahía Blanca, Argentina

Supporting Information

ABSTRACT: We report the use of bis-catecholic polymers as candidates for obtaining effective, tunable gatekeeping coatings for mesoporous silica nanoparticles (MSNs) intended for drug release applications. In monomers, catechol rings act as adhesive moieties and reactive sites for polymerization, together with middle linkers which may be chosen to tune the physicochemical properties of the resulting coating. Stable and low-toxicity coatings (pNDGA and pBHZ) were prepared from two bis-catechols of different polarity (NDGA and BHZ) on MSN carriers previously loaded with rhodamine B (RhB) as a model payload, by means of a previously reported synthetic methodology and without any previous surface modification. Coating robustness and payload content were shown to depend significantly on the workup protocol. The release profiles in a model physiological PBS buffer of coated systems (RhB@MSN@pNDGA and RhB@MSN@pBHZ) showed marked differences in the "gatekeeping" behavior of each coating, which correlated qualitatively with the chemical nature of their respective linker moieties. While the uncoated system (RhB@MSN) lost its payload almost completely after 2 days, release from RhB@MSN@pNDGA was virtually negligible, likely due to the low polarity of the parent bis-catechol (NDGA). As opposed to these extremes, RhB@MSN@pBHZ presented the most promising behavior, showing an intermediate release of 50% of the payload in the same period of time.

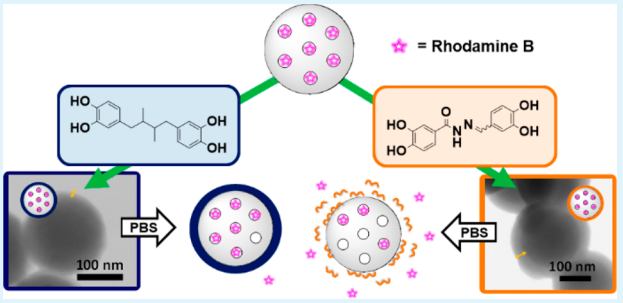

KEYWORDS: *mesoporous silica nanoparticles, polydopamine, bis-catechols, gatekeeping, biocompatible coatings*

1. INTRODUCTION

Mesoporous silica nanoparticles (MSNs) are one of the most thoroughly studied encapsulation systems in the field of nanomedicine, thanks to its large surface area and high loading capacity, excellent stability, and its simple, scalable, cost-effective, and controllable preparation procedure.[1] Yet, unmodified MSNs-based nanocarriers show potential toxicity due to interactions of surface silanols with cellular membranes,[2−4] and lower efficiency by the prerelease of loaded drug molecules during the blood circulation.[5] Because of this, surface modification strategies of MSNs are necessary to increase the circulation time.[6]

The most simple one consists of the attachment of specific payloads (therapeutic drugs, proteins, antibodies, and other nanoparticles) to the surface of MSNs, either by electrostatic interactions or covalent linkages through reaction with silanol groups.[7−10] Another established approach is based on the use of "gatekeepers", which are usually bulky molecules,[11−13] nanoparticles,[14] or polymers[15] placed on the pore outlets of previously loaded MSNs. Polymer coatings may be also formed on the surface of MSNs through noncovalent assembly or surface-initiated polymerizations.[16−19] Likewise, most of the aforementioned strategies rely on the response to external (ultrasound, light, temperature, or magnetic fields) and internal (pH, redox conditions, glucose, or enzymes) stimuli, which allow greater control and specificity of the release process.[20] In general, these stimuli lead to physical changes (solubility,

Special Issue: 10 Years of Polydopamine: Current Status and Future Directions

Received: June 14, 2017
Accepted: September 14, 2017

DOI: 10.1021/acsami.7b08584
ACS Appl. Mater. Interfaces XXXX, XXX, XXX−XXX

ionization, conformation, or swelling) of attached molecules or polymers[21,22] or rupture of the covalent bond between the gatekeeper and the MSNs.

Among all strategies, polymer coatings are particularly appealing because they allow tailor-made designs and ad hoc functionalization. For example, neutral or hydrophilic coatings not only reduce nonspecific protein adsorption but should also provide colloidal stability, preventing the aggregation of the MSNs.[23] However, in most cases surface grafting of monomers and specific conditions are required to carry out the polymerization properly. Thus, from a practical point of view, it would be desirable to devise surface treatments that are both straightforward and as widely applicable as possible.

L-DOPA, a catecholic amino acid present in mussel foot proteins in varying, but significant, amounts, was long ago identified by Waite and Tanzer as the main source for the robust and versatile wet adhesion of mussels to mineral surfaces in their native habitats[24] and, more generally, to all kinds of surfaces, even low-fouling materials such as paraffin and PTFE, in controlled laboratory experiments. In recent years, the chemistry of catechol derivatives such as dopamine has been thoroughly studied in order to exploit their full potential as universal anchors for surface modification. More specifically, since the pioneering discover by Messersmith et al.,[25] coatings based on polydopamine,[26−28] as well as on related catecholamines, such as poly(norepinephrine),[29−31] have been presented as promising coatings in the biological field due to their pH response at low pH values, biocompatibility, and low cytotoxicity. Very recently we reported how PDA coatings on MSNs can be alternatively prepared in situ by making use of a new ammonia-triggered catechol polymerization.[32,33] Besides maintaining a mildly basic pH necessary for the fast oxidation of the catechol ring under aerobic conditions, ammonia presumably acts as a nucleophile on the reactive *o*-quinones thus formed. This provides the desired covalent cross-link between adjacent catechol rings, without the need to use dopamine as constitutive monomer. In this context, bis-catechols would appear as excellent candidates for obtaining polymeric coatings on MSNs, with catechol rings acting as adhesive anchors and polymerizable sites, while using the chemical nature of the middle linking moieties in order to fine-tune its physicochemical and release profile properties.

Herein, we report the preparation and characterization of novel coating materials from two bis-catechols, *N*′-(3,4-dihydroxybenzylidene)-3,4-dihydroxybenzohydrazide (BHZ) and nordihydroguaiaretic acid (NDGA) (see Scheme 1). Stable coatings were prepared in situ on MSNs carriers previously loaded with rhodamine B (RhB) as a payload model, without previous surface modification requirements. The coating robustness and colloidal stability of the coated carriers, as well as payload content, were followed in detail throughout the coating and purification stages. Finally, removal and release profiles in a model physiological PBS buffer for the coatings and the payload were obtained, respectively, in order to assess the performance of these polymers as potential candidates for their use as gatekeeping coatings in drug delivery platforms.

Scheme 1. Chemical Structure of BHZ and NDGA Bis-catechols

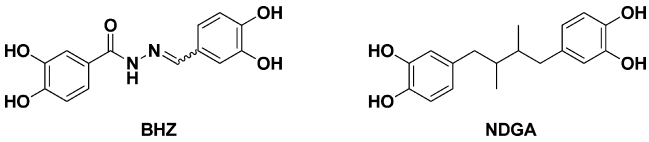

2. EXPERIMENTAL SECTION

2.1. Reagents. All chemicals were used without further purification. Tetraethyl orthosilicate (TEOS; 98%), *n*-cetyltrimethylammonium bromide (CTAB; 99%), nordihydroguaiaretic acid (NDGA; ≥97%), 3,4-dihydroxibenzaldehyde (97%), 3,4-dihydroxibenzohydrazide (97%), and rhodamine B (RhB; ≥95%) were obtained from Sigma-Aldrich. Ammonium nitrate (NH_4NO_3; 99.9%), ammonium hydroxide (NH_4OH; 28−30 wt % as NH_3), chloroform ($CHCl_3$; 99.8%), sodium hydroxide (NaOH; ≥98%), and absolute ethanol were purchased from Panreac. Methanol and acetic acid glacial were obtained from Scharlau. Ultrapure water was obtained from a Millipore Milli-Q system with a 0.2 μm pore size Milli-pak filter and used throughout for the preparation of all aqueous solutions.

2.2. Characterization Techniques. Fourier transform infrared spectroscopy (FT-IR) was carried out in a Thermo Nicolet Nexus equipped with a Goldengate attenuated total reflectance (ATR) device or in a Tensor 27 FT-IR spectrometer (Bruker) in the range of 400−4000 cm^{-1} using KBr pellets. Thermogravimetry analysis (TGA) was carried out in the 20−800 °C range at 10 °C min^{-1} in PerkinElmer Pyris Diamond TG/DTA equipment. Scanning electron microscopy (SEM) and scanning transmission electron microscopy (STEM) images were acquired on a Magellan 400L in extreme resolution mode (XHR) at 20 kV, using a carbon coated copper grid as support. STEM images and energy dispersive X-ray (EDX) line scan profiles were obtained at room temperature and 200 kV on a FEI Tecnai G2 F20 coupled to an EDAX detector. The size distribution and ζ potential of the particles were measured by dynamic light scattering (DLS) on a Zetasizer Nano 3600 instrument (Malvern Instruments, U.K.) at 37 °C on samples diluted at 0.1 mg/mL. UV−vis spectroscopy was carried out on a Cary 60 spectrophotometer in the 300−800 nm range. Fluorescence emission was measured with a Hitachi F-2500 fluorescence spectrophotometer with excitation and emission slits of 5 nm and a PMT voltage of 400 V. Fluorescence images were taken with a Zeiss Axio Observer Z1m optical microscope in reflectance mode and in fluorescence mode with an Alexa Fluor 546 filter.

2.3. Pore Size Measurements. Porosity was determined by N_2 sorption on a Micromeritics ASAP 2020, previously degassing samples under vacuum for 24 h at room temperature. The surface area was determined using the Brunauer−Emmett−Teller (BET) method and the pore volume, V_{pore} (cm^3/g), was estimated from the amount of N_2 adsorbed at a relative pressure around 0.99. The pore size distribution between 0.5 and 40 nm was calculated from the desorption branch of the isotherm by means of the Barrett−Joyner−Halenda (BJH) method. A mesopore size of 2.6 nm for the MSNs was determined from the peak of the pore size distribution curve.

2.4. Statistical Analysis. ANOVA multivariate analysis were carried out on R, an open statistics software,[34] choosing a 95% significance level ($p \leq 0.05$). Tukey's HSD and Fisher's least significant difference (LSD) tests were performed as post hoc analysis for pairwise differences. LSD test was carried out using the "*agricolae*" package in R.

2.5. Quantification of RhB. RhB content in aliquots extracted from reaction mixtures, workup washes, degradation, and release profile studies was determined by UV−vis and fluorescence spectroscopies. For UV−vis, calibration curves were fit for solutions of RhB in the 0.25−10 ppm range for different media: pure water; a model physiological 2 mM PBS buffer (pH 7.0) containing 150 mM NaCl as electrolyte; *i*-PrOH/NH_3; and EtOH. For fluorescence measurements, signal calibration was carried out in the model physiological PBS buffer in the range of 25−150 ppb by recording emission at the 573 nm maximum (λ_{exc} = 554 nm).

2.6. Synthesis of Mesoporous Silica Nanoparticles. To a 500 mL round-bottom flask, 0.5 g of CTAB as a structure-directing agent, 240 mL of H_2O (Milli-Q), and 1.75 mL of NaOH (2 M) were added. The mixture was heated to 80 °C at 600 rpm, and 12.2 mmol of TEOS

DOI: 10.1021/acsami.7b08584
ACS Appl. Mater. Interfaces XXXX, XXX, XXX−XXX

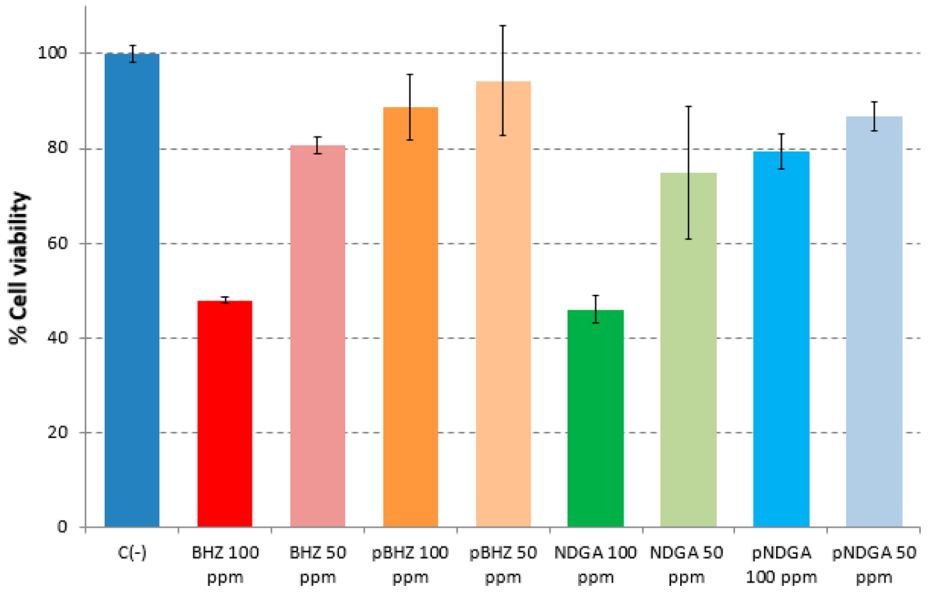

Figure 1. Cell viability of HOS cells treated with BHZ, NDGA, and their respective polymerized products pBHZ and pNDGA at concentrations of 50 and 100 ppm.

was added dropwise at 0.25 mL/min. The white suspension obtained was further stirred for 2 h at 80 °C, filtered, and washed with 50 mL of H_2O and 3 × 50 mL of EtOH. Finally, the surfactant was removed by ion exchange at 65 °C under magnetic stirring overnight, with a solution of ammonium nitrate (10 mg/mL) in 175 mL of ethanol (95%), The white solid obtained was washed three times with EtOH and dried under vacuum.

2.7. Synthesis of BHZ. 3,4-Dihydroxybenzaldehyde (1 mmol, 138 mg) and 3,4-dihydroxybenzahydrazide (1 mmol, 168 mg) were dissolved in 25 mL of methanol. A 50 μL aliquot (0.9 mmol) of glacial acetic acid was then added, and the reaction was stirred overnight at room temperature. The solvent was evaporated under vacuum, and the solids were washed and filtered with diethyl ether, yielding the final product as a yellowish powder (88%). ^{1}H NMR (DMSO-d_6): δ 11.32 (br s, NH), 9.58 (s, OH), 9.34 (s, OH), 9.25 (s, OH), 9.20 (s, OH), 8.21 (s, CH_{iminic}), 7.33 (d, J = 2.0 Hz, 1H), 7.26 (dd, J_1 = 8.2 Hz, J_2 = 2.0 Hz, 1H), 7.21 (d, J = 1.6 Hz, 1H), 6.89 (dd, J_1 = 8.1, J_2 = 1.6 Hz, 1H), 6.80 (d, J = 8.2 Hz, 1H), 6.77 (d, J = 8.1 Hz, H). ^{13}C NMR (MeOD): δ 165.5, 149.3, 149.0, 148.1, 145.4, 145.1, 126.1, 124.0, 121.2, 119.6, 114.8, 114.7, 114.6, 112.7. IR (KBr pellet; cm^{-1}): ν 3600−3000 (st, O−H), 1590 (st N = C/C = C), 1493 (st, N = C), 1269 (st, C−O).

2.8. Synthesis of pBHZ/pNDGA. BHZ or NDGA (0.1 mmol, 29 mg, and 30 mg respectively) was dissolved in 13 mL of isopropanol, and aqueous NH_3 (25 wt %, 10 mmol, 0.75 mL) was added to initiate the polymerization reaction. The reaction was kept under magnetic stirring at 45 °C for 24 h. The final product (pBHZ or pNDGA, respectively) was centrifuged and washed successively with 3 mL of water and 3 mL of EtOH.

2.9. Synthesis of MSN@pBHZ/MSN@pNDGA. In a typical reaction, BHZ or NDGA (0.1 mmol, 29 mg and 30 mg respectively) was dissolved in 13 mL of isopropanol. To the previous solution, 10 mg of MSNs and aqueous NH_3 (25 wt %, 10 mmol, 0.75 mL) were added. The suspension was kept under magnetic stirring at 45 °C for 24 h. The final products MSN@pBHZ (MSNs coated with pBHZ polymer) and MSN@pNDGA (MSNs coated with pNDGA polymer) were centrifuged and washed successively with 3 mL of water and 3 mL of EtOH.

2.10. Synthesis of RhB@MSNs. A 30 mg amount of MSNs was added to 8 mL of an aqueous solution of RhB (1 mg/mL) and left under magnetic stirring at 37 °C for 48 h. RhB@MSNs were then centrifuged and washed with 5 × 8 mL of miliQ water. Quantification of the final loading of RhB in the MSNs was carried out analyzing all supernatants by UV−vis spectroscopy and subtracting the combined amounts of RhB in these, from the initial amount of RhB in the reaction mixture.

2.11. Synthesis of RhB@MSN@coating. BHZ or NDGA (0.15 mmol, 43 mg, or 45 mg, respectively) was dissolved in 20 mL of isopropanol, and aqueous NH_3 (25 wt %, 15 mmol, 1 mL) was added dropwise. The solution was heated at 45 °C and stirred for 2 h, after which the mixture was cooled to 0 °C with an ice bath. A 10 mg amount of RhB@MSNs was then added to the mixture and stirred for 1 h at 0 °C. The temperature was increased again to 45 °C, and the suspension was finally stirred for 20 h to complete the deposition of the coating.

2.12. Coating Removal from MSNs. Coating removal was followed in pure water and in the model PBS buffer. A 10 mg amount of MSN@coating (pBHZ, pNDGA) was dispersed in 1.5 mL of the corresponding test medium (water or PBS buffer) and kept under magnetic stirring at 37 °C. Aliquots of 50 μL were taken from the dispersion at given time intervals and centrifuged at 10000 rpm for 2 min. Solid residues containing the coated MSNs were dried, and the remainder coatings were analyzed by FT-IR and STEM.

2.13. Release Studies of RhB. Tests were carried out in forced release conditions. 5 mg of RhB@MSNs, RhB@MSN@pBHZ, or RhB@MSN@pNDGA were dispersed in an Eppendorf vial in 1.5 mL of PBS buffer and kept at 37 °C under magnetic stirring for 2 days. In order to record the release profile, 1 mL aliquots were taken at given time intervals, centrifuged at 2000 rpm at 0 °C and passed through 0.2 μm pore size acetyl cellulose syringe filters to exclude any residual particles. After each extraction, the test sample was refilled with fresh PBS buffer in order to make up for the extracted volume of liquid.

2.14. HOS Cell Viability Assays. Human osteosarcoma cancer cell lines (HOS) were seeded in a concentration of 4 × 10^4 cells/well in two 12-well plates during 24 h at 37 °C and 5% CO_2 to reach confluence in each cell plate. The cultures were carried out in Dulbecco's modified Eagle's medium (DMEM) completed with fetal bovine serum and antibiotic. After those 24 h, the medium was removed and the cells were washed twice with PBS 1×. Thereafter, solutions of the BHZ, NDGA, pBHZ, or pNDGA were added to the cell culture to be studied at two different concentrations (50 and 100 μg/mL) in DMEM. After 24 h, the monomers' and polymers' solutions were removed and the cells washed twice with PBS (1×) and MTS aqueous reagent solution was then pipetted into each well in order to determinate the cell viability. To that end, samples were incubated for 4 h at 37 °C and 5% CO_2 under dark conditions and, then, the absorbance of the samples medium was measured at 460 nm using a Helios Zeta UV−vis spectrophotometer.

DOI: 10.1021/acsami.7b08584
ACS Appl. Mater. Interfaces XXXX, XXX, XXX−XXX

3. RESULTS AND DISCUSSION

3.1. Synthesis and Characterization of MSN@pBHZ and MSN@pNDGA. The oxidative polymerization of BHZ or NDGA in aqueous ammonia (see Experimental Section), afforded the respective catecholic polymers after 24 h, either as standalone materials or as well-defined, uniform, and reproducible coatings when MSNs were added to the reaction medium. To further evaluate the potential of these materials for biomedical applications, HOS cells were exposed to different concentrations of BHZ, pBHZ, NDGA, and pNDGA. Cytotoxicity was evaluated by MTS viability protocol for cell death determination. Static cell studies showed that samples exposed to BHZ and NDGA presented higher toxicity than the respective polymers (pBHZ and pNDGA), which displayed cell viability around 90% and 80%, respectively, at concentrations of 100 μg/mL. At lower concentrations (50 μg/mL), higher viability was observed both with free and polymerized monomers. Overall, these results confirmed the low toxicity of these novel bis-catechol-based polymers and their viability to be used as effective coatings for drug delivery carriers (Figure 1).

In coated systems (MSN@pBHZ and MSN@pNDGA), the presence of the corresponding ultrathin coatings was confirmed by STEM and EDX scan profiles across sections of nanoparticles, which showed carbon signals peaking at the edges of the silica core. Both STEM and EDX results were in agreement with MSN@coating core−shell structures, where pBHZ and pNDGA polymer shells showed average thicknesses of 20−24 and 8−12 nm, respectively (Figure 2a).

Since pNDGA coatings were thinner than pBHZ and gave less contrast in STEM images, HRSEM was used to confirm unambiguously their presence in MSN@pNDGA (Supporting Information Figure S1). For both MSN-coated systems, the presence of the corresponding polymers was also observed in FT-IR spectra (Supporting Information Figure S2), where characteristic bands for each catecholic compound were clearly visible alongside those of the silicon dioxide. The quantification of the organic fraction in the coated systems was done by TGA, where catecholic coatings were shown to amount to 32% in MSN@pBHZ and 36% in MSN@pNDGA (Supporting Information Figure S3).

DLS of the uncoated MSNs in model physiological PBS buffer showed particle diameters of 235 ± 90 nm, similar to those observed by STEM (Supporting Information Figure S4). For coated systems (MSN@pBHZ and MSN@pNDGA), some aggregation was observed in the PBS buffer, where the average size increased to 600−800 nm (data not shown). This could be reversed by the addition of a 30 mg/mL aqueous stock solution of BSA, which, according to reported results,[35,36] affords the formation of a protective protein corona around the NPs. In this way, both MSN@pBHZ and MSN@pNDGA were properly stabilized in the dispersion medium, showing mean sizes of 295 ± 32 and 271 ± 30 nm, respectively.

Surface charge measurements also revealed significant differences between uncoated and coated systems (Figure 2b). The former showed ζ potential values in model PBS buffers of −11, −8, and ∼0 mV, at pH 8.0, 7.0, and 5.8, respectively. On the other hand, the surface charge in coated systems (MSN@pBHZ and MSN@pNDGA) took mean values of −18, −15, and −13 mV at the same respective pHs, i.e., higher in all cases than those observed for uncoated MSNs and, remarkably, quite similar to each other, regardless of the nature

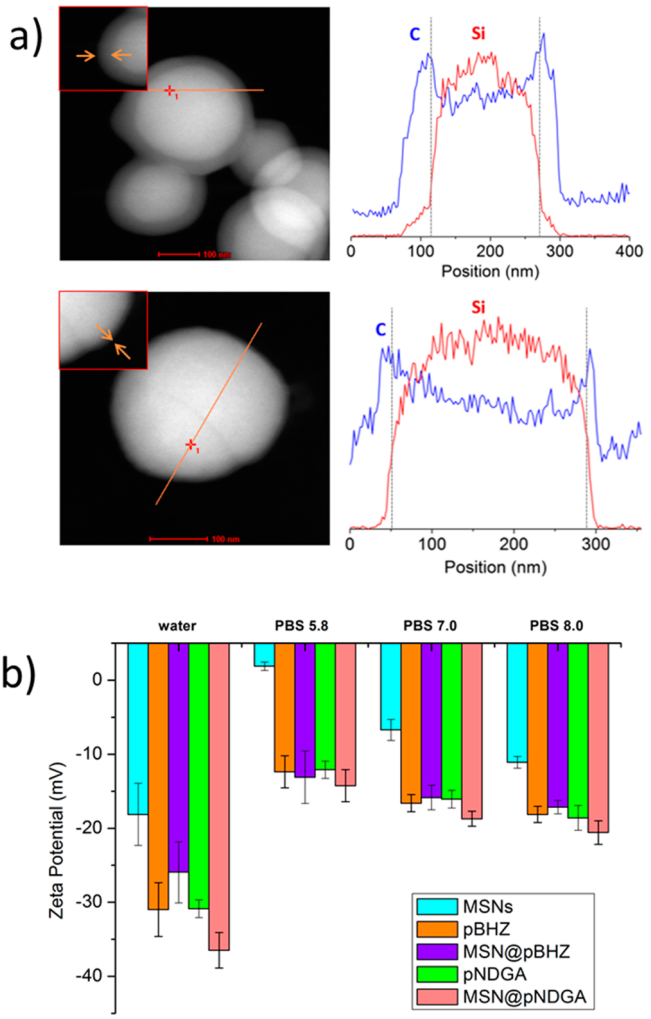

Figure 2. (a) STEM images and EDX line scan profiles across sections of MSN@pBHZ (top) and MSN@pNDGA (bottom) nanoparticles. Scale bars = 100 nm. (b) Dependence of ζ potential with pH of uncoated MSNs, nanostructured pBHZ and pNDGA, and coated MSN@pBHZ and MSN@pNDGA systems.

of the coating. These results thus indicate that the silica surface is effectively shielded by the polymeric shell in coated systems, where catechol moieties on the surface would be mostly responsible for the observed net surface charge.

3.2. Optimization of the Coating Process for MSN@pBHZ. To gain better insight into the formation of these coatings, the polymerization reaction was optimized using MSN@pBHZ as a model system, since the growth of the coating could be adequately followed by STEM for this family of coated MSNs, as discussed previously. We started by studying the influence of temperature and initial concentration of bis-catechol, as these are considered to be the main parameters affecting the growth of related polydopamine (PDA) coatings.[37,38] A first set of experiments addressed the effect of the reaction temperature on the final coating. STEM images of the final product showed that whereas no coating was observed at 20 °C, homogeneous coatings were obtained at 45 °C (Supporting Information Figure S5). In a second group of experiments, four different initial concentrations of bis-catechol were studied (0.7, 3.5, 7.0, and 14.0 mM). STEM images revealed that most MSNs remained uncoated or showed incomplete coating for bis-catechol concentrations up to 3.5

DOI: 10.1021/acsami.7b08584
ACS Appl. Mater. Interfaces XXXX, XXX, XXX−XXX

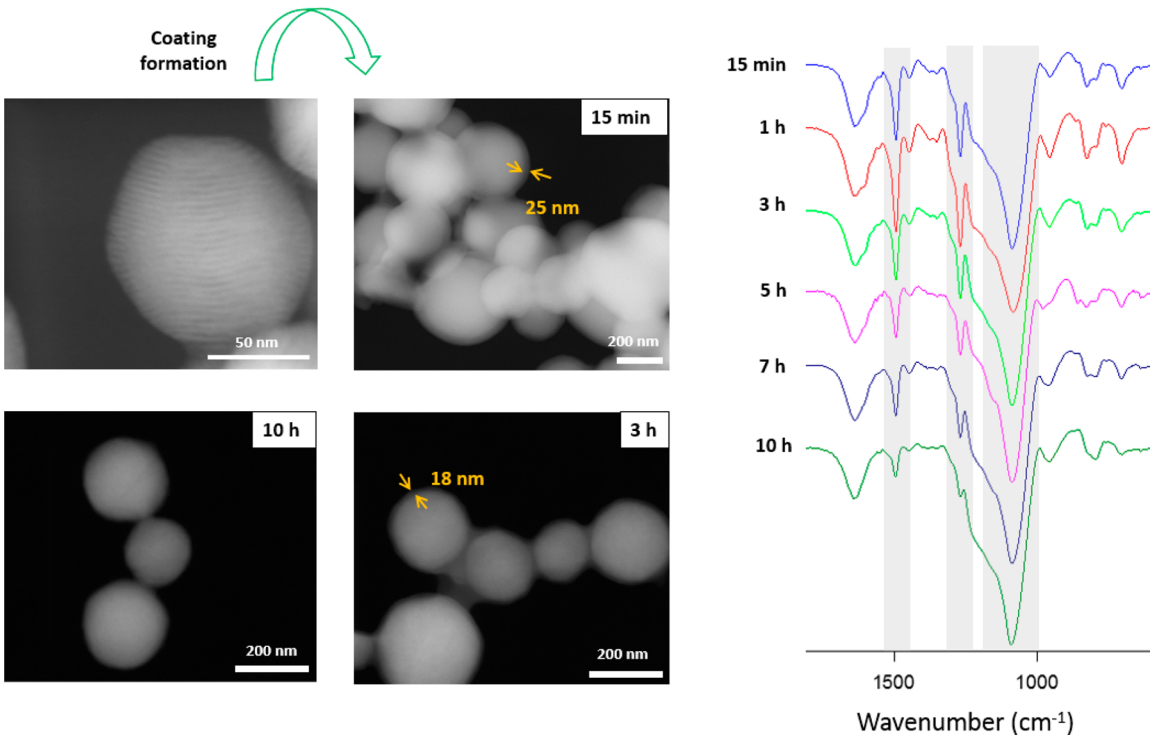

Figure 3. STEM images of MSN@pBHZ nanoparticles upon exposure to the PBS buffer at different time intervals. After 10 h, the coating cannot be observed any more (left). FT-IR spectra of MSN@pBHZ showing the progressive removal of the pBHZ coating upon exposure to the PBS buffer (right).

mM (Supporting Information Figure S6). A concentration of 7.0 mM was considered optimal, affording well-defined and homogeneous coatings, whereas higher bis-catechol concentrations induced the undesired formation of aggregates.

In subsequent experiments, three additional parameters were varied independently: (i) reaction time, (ii) stirring rate, and (iii) postsynthetic washes. For each case, STEM images were obtained from 20 to 30 different, separate areas of the sample. In all images, the coating thickness was measured for each coated MSN system and the combined values were represented as a function of particle size. Finally, multivariate ANOVA was used to estimate the independent effect of each of the three variables under control on coating thickness, taking particle size into account.

Results show no significant differences in coating thickness when reaction time is increased from 24 to 48 h (Supporting Information Figure S7). This is reminiscent of a similar phenomenon earlier observed for PDA coatings, the growth of which stops, even in the presence of polymer in the mixture, after self-aggregation of the prepolymer becomes dominant over deposition on the substrate.[39] Regarding magnetic stirring rates, experiments carried out at 50, 140, 300, and 500 rpm suggest that while MSNs size would not affect coating thickness, this increases with stirring rate, although a change of at least 1 order of magnitude of this parameter is needed in order to show a significant effect (Supporting Information Table S1 and Figure S8).

Finally, since the workup protocol should be devised as to minimize undesired leakage of the payload from the loaded nanoparticles, the effect of postsynthesis washes was assessed for both coated systems. For MSN@pBHZ, a batch was divided into three different fractions, washed with water one, two, or three times, respectively. p-values of 0.393 and 10^{-16} for the effect of particle size and number of washes, respectively, showed that postwash coating thickness did not depend on particle size but was otherwise strongly dependent on the number of washes. In this case, Tukey's test determined that all data pairs were significantly different, with the exception of the two-wash/three-wash pair, indicating that only the two first washes reduce coating thickness significantly. The same experiment was carried out washing MSN@pBHZ with ethanol instead of water (Supporting Information Figure S9). For this solvent, p-values of 0.098 for particle size and 0.866 for the number of ethanol washes indicated no significant impact of either parameter on the final coating thickness. Overall, water washes turned out to be more efficient than ethanol in removing loosely bound layers of this polymeric coating.

For MSN@pNDGA, protocols using different washing solvents (2 × water; 2 × ethanol; 1 × ethanol followed by 1 × water) were cross-tested (Supporting Information Figure S10). Statistical analysis afforded a p-value of 10^{-12} for the effect of the washing procedure and 0.270 for particle size, confirming again the lack of relevance of the latter in determining coating thickness. With regard to the washing procedure, Tukey's test determined that all pairs were significantly different, except the one formed by 2 × water/no washes. Thus, while water washes did not alter this hydrophobic coating significantly, even a single ethanol wash did. Overall, results were qualitatively in accordance with differences in polarity and solubility of the bis-catecholic monomers (NDGA is completely insoluble in water and soluble in EtOH, whereas BHZ is somewhat soluble in both), which would be expected to show, at least to some degree, in their respective polymers (pBHZ and pNDGA) (Supporting Information Figure S11).

DOI: 10.1021/acsami.7b08584
ACS Appl. Mater. Interfaces XXXX, XXX, XXX−XXX

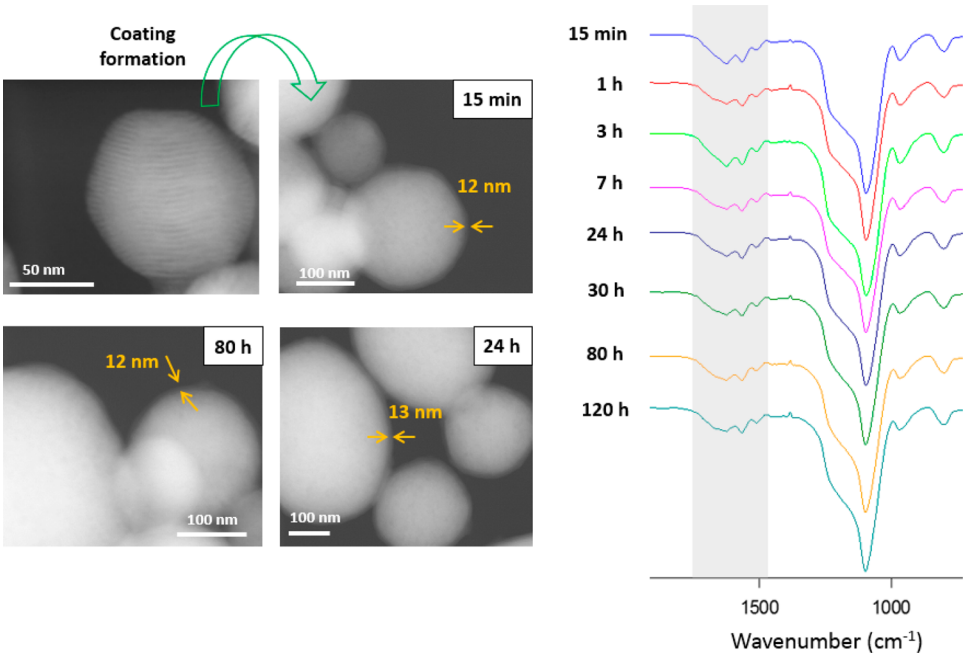

Figure 4. STEM images of MSN@pNDGA nanoparticles upon exposure to the PBS buffer at different time intervals. Coating thickness remains essentially unchanged (left). FT-IR spectra of MSN@pNDGA showing the persistence of the pNDGA coating upon exposure to the PBS buffer (right).

3.3. Coating Stability in Aqueous Media. Removal of the polydopamine coating from MSN@pBHZ, both in PBS buffer and in water, was followed by FT-IR analysis (Figure 3 and Supporting Information Figure S12, respectively), showing a decrease in the ratio of intensities of the characteristic peaks of the catecholic compound (1493 and 1269 cm^{-1}, respectively), with regard to those of the silica core (1084 cm^{-1}). The evolution of the coating thickness followed by STEM was seen to be in qualitative agreement with FT-IR data. Overall, removal was virtually complete after 10 h of contact with either aqueous medium. In stark contrast with pBHZ, pNDGA coatings showed virtually no removal after 80 h in the same aqueous media (Figure 4 and Supporting Information Figure S13, respectively), since thickness remained essentially unchanged over several days. FT-IR spectra confirmed the persistence of pNDGA coatings in MSN@pNDGA, even after 4 days.

3.4. Preparation and Coating of RhB@MSNs with pBHZ and pNDGA. In order to minimize the premature release of the cargo from previously loaded RhB@MSNs nanoparticles, the deposition of pBHZ and pNDGA coatings was carried out in three stages. First, the polymerization of the catecholic monomer was initiated at a relatively high temperature (45 °C) for a given period of time. Before the addition of the loaded carrier, the temperature was decreased in order to minimize the unintended release of RhB from the MSNs, worsened by the basicity of the reaction medium, while at the same time allowing the deposition of an incipient polymer layer on top. Finally, the temperature was raised again in order to consolidate the growth of the polymer layer. In this way, dye-loaded coated nanoparticles RhB@MSN@pBHZ and RhB@MSN@pNDGA were successfully prepared from a single batch of RhB@MSNs with a 5.3 wt % payload. The presence of RhB in loaded systems, both before and after coating, was confirmed by fluorescence microscopy (λ_{ex} = 540−542 nm, λ_{em} > 590 nm; Supporting Information Figures S14 and S15). Taking into account the influence of postsynthesis washes observed previously on the coating thickness of unloaded systems, special care was taken to study the effect of workup on the final loading of RhB. For this, RhB@MSN@pBHZ samples were washed five times with ethanol, while those of RhB@MSN@pNDGA were washed three times with water, measuring the amount of RhB leached with each wash. Whereas RhB was barely detectable in the supernatant of the third wash of the RhB@MSN@pNDGA system, RhB@MSN@pBHZ showed a very different behavior, with the payload still detectable in the fifth wash. Since the effect of washes might hint at the physical distribution of the payload (either inside the MSN pores, entrapped within the pBHZ shell, or both),[4] a batch of ∼200 nm nonporous SiO_2 NPs, obtained by Stöber's method according to an optimized protocol,[40] was put in contact with a RhB solution and further coated with pBHZ, using the same procedure used for mesoporous systems and its behavior compared to that of RhB@MSN@pBHZ. As shown in Figure S16, RhB was quantitatively removed from SiO_2@RhB-pBHZ after just four EtOH washes. This suggests that payload loss during the first four washes of the coated mesoporous system (RhB@MSN@pBHZ) came mainly from the outer pBHZ shell, where RhB is presumably entrapped in significant amounts, whereas removal of the payload from the pores would be the main operating mechanism in further washes. Overall, the final payload contents after washing were 1.2 and 1.9 wt % for RhB@MSN@pBHZ and RhB@MSN@pNDGA, respectively. Although modest, these values were high enough to further follow the release procedure by spectroscopic techniques.

3.5. Release Profiles of RhB from RhB@MSN@pBHZ and RhB@MSN@pNDGA. As a proof of concept for the use of these novel catechol-based coatings for drug delivery, we studied the release profiles of rhodamine B from coated MSN systems (RhB@MSN@pBHZ and RhB@MSN@pNDGA) in the model PBS buffer and compared them with that of the uncoated carrier (RhB@MSNs) (Figure 5). Tests were carried

DOI: 10.1021/acsami.7b08584
ACS Appl. Mater. Interfaces XXXX, XXX, XXX−XXX

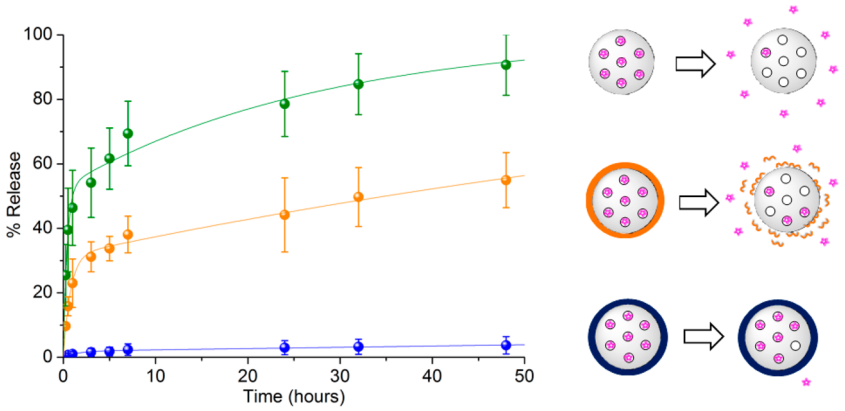

Figure 5. Experimental data corresponding to the release profiles of RhB from (green ●) RhB@MSNs, (orange ●) RhB@MSN@pBHZ, and (blue ●) RhB@MSN@pNDGA and their corresponding model fitting curves for (green —) RhB@MSNs, (orange —) RhB@MSN@pBHZ, and (blue —)RhB@MSN@pNDGA.

Table 1. Release Mode Contributions and Kinetic Parameters Fitted from the Experimental Release Profiles of the Uncoated (RhB@MSN) and Coated (RhB@MSN@pBHZ, RhB@MSN@pNDGA) Systems

	A_1 (%)	A_2 (%)	k_s (h^{-1})	k_{on} (10^3 h^{-1})	k_{off} (10^3 h^{-1})	R^2
RhB@MSN	52.7	47.3	2.427	30.9	36.5	0,9819
RhB@MSN@pBHZ	31.5	68.5	1.286	19.2	9.1	0,9938
RhB@MSN@pNDGA	1.9	98.1	0.618	20.3	0.4	0,9846

out in forced release conditions, reducing the external concentration of RhB, inducing its release as could happen in physiological conditions through a high concentration difference in the bloodstream. Whereas uncoated MSNs (RhB@MSNs) showed a relatively fast payload release, reaching a value around 90% after 48 h, dye release in the RhB@MSN@pNDGA system was negligible throughout the same period of time. In turn, RhB@MSN@pBHZ showed an intermediate behavior, with a release of around 50% of the payload.

Release profiles were analyzed using a theoretical three-parameter model previously developed to explain the release kinetics from nanocarriers in general,[41] which has recently been applied to MSNs loaded with a model drug.[42] This model factors the cumulative percent release in two main contributions, each modeled by means of an exponential term, the first one corresponding to the initial burst (governed by a relative contribution, A_1, and a time constant, λ_1) and the other to an underlying, sustained release (parametrized by A_2 and λ_2). Assuming first order kinetics, constants for the diffusion of the payload into the suspension medium (k_S), and those describing the payload−carrier interaction in terms of reversible association (k_{on}) and dissociation (k_{off}) processes may be derived analytically from the following equations:

$$\%\ \text{release} = A_1(1 - e^{-\lambda_1 t}) + A_2(1 - e^{-\lambda_2 t}) = \frac{\lambda_2(k_S - \lambda_2)}{(k_{on} + k_{off})(\lambda_1 - \lambda_2)}(1 - e^{-\lambda_1 t}) + \frac{\lambda_1(\lambda_1 - k_S)}{(k_{on} + k_{off})(\lambda_1 - \lambda_2)}(1 - e^{-\lambda_2 t})$$

where

$$\lambda_{1,2} = [(k_s + k_{on} + k_{off} \pm \sqrt{(k_S + k_{on} + k_{off})^2 - 4k_S k_{off}}\,] / 2$$

This model gives very good fittings for the release profiles of all three systems (see Table 1). In accordance with a previously reported classification for drug release profiles,[43] all systems show a type III release, but with important differences of degree: while both RhB@MSN and RhB@MSN@pBHZ show fast burst releases—where $\lambda_1 \cong k_S$—their quantitative contributions to the total release are significatively different (53% vs 32%, respectively). Moreover, the sustained release rate, which may be approximated by $\lambda_2 \cong k_{off}$, is four times slower for RhB@MSN@pBHZ compared to the uncoated control. With regard to RhB@MSN@pNDGA, the burst release contribution, although still fast, is almost completely suppressed (<2%).

The estimated values for k_{on} and k_{off} hint at different behaviors regarding the interaction between the payload, the coating (if present), and the mesoporous carrier. For the uncoated system RhB@MSN, these constants may be directly related to the combined contributions of the association/dissociation with/from the carrier, as well as the self-association of the adsorbed payload, as reported previously.[41] In coated systems, the retention or "plug" effect of the respective coatings is expected to add significantly to the former base effects. For all three systems, both constants show a decreasing pattern RhB@MSN > RhB@MSN@pBHZ > RhB@MSN@pNDGA, but this trend becomes particularly steep for the latter desorption constant, which is roughly 2 orders of magnitude lower than those of the other systems. Qualitatively, this indicates that the desorption of the payload from RhB@MSN@pNDGA is severely impeded by the coating, showing that this is likely the main effect behind the effective suppression of the burst release and the nearly flat subsequent release response. This may also be shown by equilibrium constant associated to the overall absorption/desorption process, which is given by $K_{a/d} = k_{on}/k_{off}$. Compared with the uncoated system, desorption is slightly unfavorable for RhB@MSN@pBHZ—as would correspond to a moderate retention effect—whereas it is very unfavorable in the case of RhB@MSN@pNDGA. Overall, it is shown that the kinetics of the separate processes slow down either slightly (RhB@MSN@pBHZ) o dramatically (RhB@MSN@pNDGA) with regard to the uncoated control, depending on the coating.

DOI: 10.1021/acsami.7b08584
ACS Appl. Mater. Interfaces XXXX, XXX, XXX−XXX

These results are qualitatively in accordance with the chemical natures of the respective coatings. Because of the relative hydrophobicity of the alkyl linker in the parent monomer, pNDGA showed poor affinity with water, providing a robust coating that is essentially impervious to aqueous media, and thus largely preventing payload extraction/release. On the other hand, pBHZ would show more permeability to water, likely due to the more hydrophilic nature of the hydrazone group in the linker, while still affording a sustained release of the payload. In fact, as observed in the pBHZ degradation studies (section 3.3), contact with water affected the final coating of pBHZ considerably. In any case, pBHZ afforded distinctive midterm retention of the payload, which was still present in sizable amounts within the MSNs by the time that the release of the payload from the uncoated (control) system was virtually complete.

4. CONCLUSION

In summary, we reported the synthesis and characterization of two novel and biocompatible catechol-based coatings, each obtained by ammonia-triggered polymerization of a bis-catechol, and investigated their use for drug delivery in a model system that uses MSNs as an inert payload carrier. A detailed study of the protocol of preparation of the corresponding coated systems brought to light the importance of the choice of the chemical nature of the catecholic parent monomer and synthesis post-treatment on the quality and persistence of the coatings, as well as on their release profile. As a proof of concept, we evaluated the release profile of the two coated systems in a physiological buffer, taking RhB as a model compound. Whereas pNDGA coated MSNs and an uncoated control showed opposed and extreme behaviors—the former offering negligible sustained long-term release and robust persistence of the coating in a physiological buffer and the latter releasing most of its cargo in just a few hours—pBHZ coated MSNs afforded an intermediate behavior with a moderate sustained release. Together with this, the low cytotoxicity shown by pBHZ would make this bis-catecholic polymer a good potential candidate for biomedical applications.

■ ASSOCIATED CONTENT

Supporting Information

The Supporting Information is available free of charge on the ACS Publications website at DOI: 10.1021/acsami.7b08584.

Details regarding additional characterization of MSNs@pBHZ and MSN@pNDGA, optimization and statistical studies about the coatings, degradation studies of the coatings from MSN@pBHZ and MSN@pNDGA in water, characterization of RhB@MSNs and its coated homologues, and comparative effect of washes (PDF)

■ AUTHOR INFORMATION

Corresponding Authors

*(D.R.-M.) E-mail: dani.ruiz@icn2.cat.
*(F.N.) E-mail: fabiana.nador@uns.edu.ar.

ORCID

Miguel-Ángel Moreno-Villaécija: 0000-0003-2410-0682
Alejandro Baeza: 0000-0002-9042-8865
Daniel Ruiz-Molina: 0000-0002-6844-8421

Author Contributions

All authors have given approval to the final version of the manuscript. The manuscript was written through contributions of all authors. M.-Á.M.-V. did most of the experimental work for the catechol coating. A.B. and E.G. prepared and characterized the MSNs and ran the biocompatibility studies. J.S.-V. and M.-Á.M.-V. carried out all the statistical studies and model fittings for the release profiles. D.R.-M., F.N., and M.V.R. coordinated and supervised the experimental work.

Funding

This work was supported by Projects MAT2015-70615-R from the Spanish Government and by FEDER funds. ICN2 acknowledges support from the Severo Ochoa Program (MINECO, Grant SEV-2013-0295) and the CERCA Programme/Generalitat de Catalunya. UCM acknowledges support by the European Research Council (Advanced Grant VERDI; ERC-2015-AdG Proposal No. 694160) and Project MAT2015-64831-R.

Notes

The authors declare no competing financial interest.

■ ABBREVIATIONS

BHZ, *N*′-(3,4-dihydroxybenzylidene)-3,4-dihydroxybenzohydrazide
MSNs, mesoporous silica nanoparticles
NDGA, nordihydroguaiaretic acid
PDA, polydopamine
RhB@MSNs, mesoporous silica nanoparticles loaded with rhodamine B

■ REFERENCES

(1) Tang, F.; Li, L.; Chen, D. Mesoporous Silica Nanoparticles: Synthesis, Biocompatibility and Drug Delivery. *Adv. Mater.* **2012**, *24*, 1504−1534.
(2) Lin, Y.-S.; Haynes, C. L. Impacts of Mesoporous Silica Nanoparticle Size, Pore Ordering, and Pore Integrity on Hemolytic Activity. *J. Am. Chem. Soc.* **2010**, *132*, 4834−4842.
(3) Zhao, Y.; Sun, X.; Zhang, G.; Trewyn, B. G.; Slowing, I. I.; Lin, V. S.-Y. Interaction of Mesoporous Silica Nanoparticles with Human Red Blood Cell Membranes: Size and Surface Effects. *ACS Nano* **2011**, *5*, 1366−1375.
(4) Singh, N.; Karambelkar, A.; Gu, L.; Lin, K.; Miller, J. S.; Chen, C. S.; Sailor, M. J.; Bhatia, S. N. Bioresponsive Mesoporous Silica Nanoparticles for Triggered Drug Release. *J. Am. Chem. Soc.* **2011**, *133*, 19582−19585.
(5) Zhang, Y.; Ang, C. Y.; Li, M.; Tan, S. Y.; Qu, Q.; Luo, Z.; Zhao, Y. Polymer-Coated Hollow Mesoporous Silica Nanoparticles for Triple-Responsive Drug Delivery. *ACS Appl. Mater. Interfaces* **2015**, *7*, 18179−18187.
(6) Baeza, A.; Colilla, M.; Vallet-Regí, M. Advances in Mesoporous Silica Nanoparticles for Targeted Stimuli-Responsive Drug Delivery. *Expert Opin. Drug Delivery* **2015**, *12*, 319−337.
(7) Li, Z.-Y.; Liu, Y.; Wang, X.-Q.; Liu, L.-H.; Hu, J.-J.; Luo, G.-F.; Chen, W.-H.; Rong, L.; Zhang, X.-Z. One-Pot Construction of Functional Mesoporous Silica Nanoparticles for the Tumor-Acidity-Activated Synergistic Chemotherapy of Glioblastoma. *ACS Appl. Mater. Interfaces* **2013**, *5*, 7995−8001.
(8) Giri, s.; Trewyn, B. G.; Stellmaker, M. P.; Lin, V. S.-Y. Stimuli-Responsive Controlled-Release Delivery System Based on Mesoporous Silica Nanorods Capped with Magnetic Nanoparticles. *Angew. Chem., Int. Ed.* **2005**, *44*, 5038−5044.
(9) Deng, Z.; Zhen, Z.; Hu, X.; Wu, S.; Xu, Z.; Chu, P. K. Hollow Chitosan-Silica Nanospheres as pH-Sensitive Targeted Delivery Carriers in Breast Cancer Therapy. *Biomaterials* **2011**, *32*, 4976−4986.

DOI: 10.1021/acsami.7b08584
ACS Appl. Mater. Interfaces XXXX, XXX, XXX−XXX

(10) Ferris, D. P.; Lu, J.; Gothard, C.; Yanes, R.; Thomas, C. R.; Olsen, J. C.; Stoddart, J. F.; Tamanoi, F.; Zink, J. I. Synthesis of Biomolecule-Modified Mesoporous Silica Nanoparticles for Targeted Hydrophobic Drug Delivery to Cancer Cells. *Small* **2011**, *7*, 1816−1826.
(11) Meng, H.; Xue, M.; Xia, T.; Zhao, Y.-L.; Tamanoi, F.; Stoddart, J. F.; Zink, J. L.; Nel, A. E. Autonomous in Vitro Anticancer Drug Release from Mesoporous Silica Nanoparticles by pH-Sensitive Nanovalves. *J. Am. Chem. Soc.* **2010**, *132*, 12690−12697.
(12) Hu, C.; Yu, L.; Zheng, Z.; Wang, J.; Liu, Y.; Jiang, Y.; Tong, G.; Zhou, Y.; Wang, X. Tannin as a Gatekeeper of pH-Responsive Mesoporous Silica Nanoparticles for Drug Delivery. *RSC Adv.* **2015**, *5*, 85436−85441.
(13) Mal, N. K.; Fujiwara, M.; Tanaka, Y. Photocontrolled Reversible Release of Guest Molecules from Coumarin-Modified Mesoporous Silica. *Nature* **2003**, *421*, 350−353.
(14) Lai, C.-Y.; Trewyn, B. G.; Jeftinija, D. M.; Jeftinija, K.; Xu, S.; Jeftinija, S.; Lin, V. S.-Y. A Mesoporous Silica Nanosphere-Based Carrier System with Chemically Removable CdS Nanoparticle Caps for Stimuli-Responsive Controlled Release of Neurotransmitters and Drug Molecules. *J. Am. Chem. Soc.* **2003**, *125*, 4451−4459.
(15) Bilalis, P.; Tziveleka, L. A.; Varlas, S.; Iatrou, H. pH-Sensitive Nanogates Based on Poly(L-histidine) for Controlled Drug Release from Mesoporous Silica Nanoparticles. *Polym. Chem.* **2016**, *7*, 1475−1485.
(16) Palanikumar, L.; Choi, E. S.; Cheon, J. Y.; Joo, S. H.; Ryu, J. H. Noncovalent Polymer-Gatekeeper in Mesoporous Silica Nanoparticles as a Targeted Grug Delivery Platform. *Adv. Funct. Mater.* **2015**, *25*, 957−965.
(17) Xia, T.; Kovochich, M.; Liong, M.; Meng, H.; Kabehie, S.; George, S.; Zink, J. I.; Nel, A. E. Polyethyleneimine Coating Enhances the Cellular Uptake of Mesoporous Silica Nanoparticles and Allows Safe Delivery of siRNA and DNA Constructs. *ACS Nano* **2009**, *3*, 3273−3286.
(18) Huang, S.; Fan, Y.; Cheng, Z.; Kong, D.; Yang, P.; Quan, Z.; Zhang, C.; Lin, J. Magnetic Mesoporous Silica Spheres for Drug Targeting and Controlled Release. *J. Phys. Chem. C* **2009**, *113*, 1775−1784.
(19) Yang, Y.; Yan, X.; Cui, Y.; He, Q.; Li, D.; Wang, A.; Fei, J.; Li, J. Preparation of Polymer-Coated Mesoporous Silica Nanoparticles Used for Cellular Imaging by a "Graft-from" Method. *J. Mater. Chem.* **2008**, *18*, 5731−5737.
(20) Nguyen, C. T. H.; Webb, R. I.; Lambert, L. K.; Strounina, E.; Lee, E. C.; Parat, M.-O.; McGuckin, M. A.; Popat, A.; Cabot, P. J.; Ross, B. P. Bifunctional Succinylated ε-Polylysine-Coated Mesoporous Silica Nanoparticles for pH-Responsive and Intracellular Drug Delivery Targeting the Colon. *ACS Appl. Mater. Interfaces* **2017**, *9*, 9470−9483.
(21) Coti, K. K.; Belowich, M. E.; Liong, M.; Ambrogio, M. W.; Lau, Y. A.; Khatib, H. A.; Zink, J. Y.; Khashab, N. M.; Stoddart, J. F. Mechanised Nanoparticles for Drug Delivery. *Nanoscale* **2009**, *1*, 16−39.
(22) Liu, R.; Liao, P.; Liu, J.; Feng, P. Responsive Polymer-coated Mesoporous Silica as a pH-sensitive Nanocarrier for Controlled Release. *Langmuir* **2011**, *27*, 3095−3099.
(23) Zhu, Y.; Sundaram, H. S.; Liu, S.; Zhang, L.; Xu, X.; Yu, Q.; Xu, J.; Jiang, S. A Robust Graft-to Strategy to Form Multifunctional and Stealth Zwitterionic Polymer-Coated Mesoporous Silica Nanoparticles. *Biomacromolecules* **2014**, *15*, 1845−1851.
(24) Waite, J. H.; Tanzer, M. L. Polyphenolic Substance of Mytilus Edulis: Novel Adhesive Containing L-Dopa and Hydroxyproline. *Science* **1981**, *212*, 1038−1040.
(25) Lee, H.; Dellatore, S. M.; Miller, W. M.; Messersmith, P. Mussel-Inspired Surface Chemistry for Multifunctional Coatings. *Science* **2007**, *318*, 426−430.
(26) Wei, Y.; Gao, L.; Wang, L.; Shi, L.; Wei, E.; Zhou, B.; Zhou, L.; Ge, B. Polydopamine and Peptide Decorated Doxorubicin Loaded Mesoporous Silica Nanoparticles as a Targeted Drug Delivery System for Bladder Cancer Therapy. *Drug Delivery* **2017**, *24*, 681−691.
(27) Zheng, Q.; Lin, T.; Wu, H.; Guo, L.; Ye, P.; Hao, Y.; Guo, Q.; Jiang, J.; Fu, F.; Chen, G. Mussel-inspired Polydopamine Coated Mesoporous Silica Nanoparticles as pH-sensitive Nanocarriers for Controlled Release. *Int. J. Pharm.* **2014**, *463*, 22−26.
(28) Chang, D.; Gao, Y.; Wang, L.; Liu, G.; Chen, Y.; Wang, T.; Tao, W.; Mei, L.; Huang, L; Zeng, X. Polydopamine-based Surface Modification of Mesoporous Silica Nanoparticles as pH-sensitive Drug Delivery Vehicles for Cancer Therapy. *J. Colloid Interface Sci.* **2016**, *463*, 279−287.
(29) Kang, S. M.; Rho, J.; Choi, I. S.; Messersmith, P. B.; Lee, H. Norepinephrine: Material-Independent, Mulrifunctional Surface Modification Reagent. *J. Am. Chem. Soc.* **2009**, *131*, 13224−13225.
(30) Hong, S.; Kim, J.; Na, Y. S.; Park, J.; Kim, S.; Singha, K.; Im, G.-I.; Han, D.-K.; Kim, W. J.; Lee, H. Poly(norepinephrine): Ultrasmooth Material-Independent Surface Chemistry and Nanodepot for Nitric Oxide. *Angew. Chem., Int. Ed.* **2013**, *52*, 9187−9191.
(31) Ye, Q.; Zhou, F.; Liu, W. Bioinspired Catecholic Chemistry for Surface Modification. *Chem. Soc. Rev.* **2011**, *40*, 4244−4258.
(32) Nador, F.; Guisasola, E.; Baeza, A.; Villaecija, M. A. M.; Vallet-Regí, M.; Ruiz-Molina, D. Synthesis of Polydopamine-Like Nanocapsules via Removal of a Sacrificial Mesoporous Silica Template with Water. *Chem. - Eur. J.* **2017**, *23*, 2753−2758.
(33) Saiz-Poseu, J.; Sedó, J.; García, B.; Benaiges, C.; Parella, T.; Alibés, R.; Hernando, J.; Busqué, F.; Ruiz-Molina, D. Versatile Nanostructured Materials via Direct Reaction of Functionalized Catechols. *Adv. Mater.* **2013**, *25*, 2066−2070.
(34) The R Foundation. *R Project for Statistical Computing*; 2017. Software available online at: https://www.r-project.org/ [Accessed Jun. 10, 2017].
(35) MacCuspie, R. I. Colloidal Stability of Silver Nanoparticles in Biologically Relevant Conditions. *J. Nanopart. Res.* **2011**, *13*, 2893−2908.
(36) Larsericsdotter, H.; Oscarsson, S.; Buijs, J. Structure, Stability, and Orientation of BSA Adsorbed to Silica. *J. Colloid Interface Sci.* **2005**, *289*, 26−35.
(37) Yu, B.; Wang, D. A.; Ye, Q.; Zhou, F.; Liu, W. Robust Polydopamine Nano/Microcapsules and their Loading and Release Behaviour. *Chem. Commun.* **2009**, 6789−6791.
(38) Ball, V.; Del Frari, D.; Toniazzo, V.; Ruch, D. Kinetics of Polydopamine Film Deposition as a Function of pH and Dopamine Concentration: Insights in the Polydopamine Deposition Mechanism. *J. Colloid Interface Sci.* **2012**, *386*, 366−372.
(39) Bernsmann, F.; Ball, V.; Addiego, F.; Ponche, A.; Michel, M.; Gracio, J. J. d. A.; Toniazzo, V.; Ruch, D. Dopamine-Melanin Film Deposition Depends on the Used Oxidant and Buffer Solution. *Langmuir* **2011**, *27*, 2819−2825.
(40) Rao, K. S.; El-Hami, K.; Kodaki, T.; Matsushige, K.; Makino, K. A Novel Method for Synthesis of Silica Nanoparticles. *J. Colloid Interface Sci.* **2005**, *289*, 125−131.
(41) Zeng, L.; An, L.; Wu, X. Modeling Drug-Carrier Interaction in the Drug Release from Nanocarriers. *J. Drug Delivery* **2011**, *2011*, 1−15.
(42) Mitran, R.-A.; Matei, C.; Berger, D. Correlation of Mesoporous Silica Structural and Morphological Features with Theoretical Three-Parameter Model for Drug Release Kinetics. *J. Phys. Chem. C* **2016**, *120*, 29202−29209.
(43) Ye, M.; Kim, S.; Park, K. Issues in Long-Term Protein Delivery Using Biodegradable Microparticles. *J. Controlled Release* **2010**, *146*, 241−260.

DOI: 10.1021/acsami.7b08584
ACS Appl. Mater. Interfaces XXXX, XXX, XXX−XXX